When an active bath behaves as an equilibrium one

Shubhendu Shekhar Khali,[1,*] Fernando Peruani,[2,†] and Debasish Chaudhuri[1,3,‡]
[1]*Institute of Physics, Sachivalaya Marg, Bhubaneswar 751005, India*
[2]*LPTM, CY Cergy Paris Université, 2 Avenue A. Chauvin, 95302 Cergy-Pontoise Cedex, France*
[3]*Max-Planck Institute for the Physics of Complex Systems, Nöthnitzer Strasse 38, 01187 Dresden, Germany*

(Received 10 May 2023; revised 8 January 2024; accepted 22 January 2024; published 20 February 2024)

Active scalar baths consisting of active Brownian particles are characterized by a non-Gaussian velocity distribution, a kinetic temperature, and a diffusion coefficient that scale with the square of the active velocity v_0. While these results hold in overdamped active systems, inertial effects lead to normal velocity distributions, with kinetic temperature and diffusion coefficient increasing as $\sim v_0^\alpha$ with $1 < \alpha < 2$. Remarkably, the late-time diffusivity and mobility decrease with mass. Moreover, we show that the equilibrium Einstein relation is asymptotically recovered with inertia. In summary, the inertial mass restores an equilibriumlike behavior.

DOI: 10.1103/PhysRevE.109.024120

I. INTRODUCTION

A fluid in equilibrium can be characterized as a heat bath in terms of temperature, viscous drag, and diffusivity, obeying the Einstein relation [1]. Active Brownian particles (ABPs), under certain conditions, can constitute a similar homogeneous and isotropic (as opposed to polar) active fluid, i.e., an active scalar fluid, in the presence of local energy dissipation and self-propulsion [2–7]. A question that naturally arises is to what extent such a fluid can be characterized as an *active* heat bath, i.e., whether it satisfies some sort of fluctuation-dissipation relation. The active nature of ABPs is determined by the self-propulsion speed v_0 and the orientational diffusivity of the heading direction D_r. This leads to a persistent random motion for individual ABPs, in dimension d, characterized by a late-time active diffusivity that scales as $\frac{v_0^2}{D_r d(d-1)}$. Nonequilibrium properties of active baths are often probed in terms of tracer particle dynamics [8–11]. Early experiments in a bacterial suspension showed enhanced active diffusion of tracers [8,9]. A higher density reduces diffusivity in equilibrium [12] but increases it in a nonequilibrium bacterial bath [8]. Various theoretical techniques were used to obtain the impact of an active bath on tracer particles [13–21]. Recent works have characterized ABP systems in terms of kinetic temperature, effective diffusivity, and viscous drag as a function of changing activity [22–29]. While diffusivity and kinetic temperature increase with activity, a nonmonotonic variation of viscous drag has been predicted [26]. At the motility-induced phase separation (MIPS) of ABPs [30–32], it was shown that the kinetic temperature could vary across a steady-state system with low (high) temperature characterizing the dense (dilute) phase [24]. However, it remains unclear to what extent such a description can be developed into a coherent self-consistent picture of active fluid, given, e.g., the breaking of time-reversal symmetry and the absence of equilibrium fluctuation dissipation.

Despite tremendous progress in the study of active matter [2–6], until recently, relatively little attention was paid to the impact of inertia on the active matter except for [24,33–39]. One reason for this is the extremely short time (≈100 ns) and length scales (angstrom) for the ballistic-diffusive crossover in colloidal particles. However, for larger active elements, including birds, fish, and animals on the one hand, and artificial macrosized robots [40–42] on the other hand, inertial effects can be substantial. This paper considers a homogeneous and isotropic fluid of ABPs and probes its active bathlike characteristics. A remarkable fact emerges: not only transient behaviors but even asymptotic properties, including the effective diffusivity, kinetic temperature, and mobility at the steady state, do depend on inertial mass, in sharp contrast to a noninteracting ABP gas. Furthermore, the strong non-Gaussian distribution of velocities returns towards equilibriumlike Gaussian for large mass. Finally, with increasing mass, the deviation from the equilibrium fluctuation-dissipation relation drops sharply. In summary, while activity amplifies nonequilibrium features, increasing the inertial mass brings the fluid back to equilibrium.

II. MODEL

We consider N ABPs of mass m, moment of inertia I, and diameter σ moving in a two-dimensional rectangular box of area $L_x \times L_y$ with periodic boundary conditions (thus, density $\rho = N/L_xL_y$). The particles self-propel in directions $\hat{n}_i = (\cos\theta_i, \sin\theta_i)$ with force $\mathbf{F}_{A,i} = \gamma_t v_0 \hat{n}_i$. The heading direction,

*shubhendu.k@iopb.res.in
†fernando.peruani@cyu.fr
‡debc@iopb.res.in

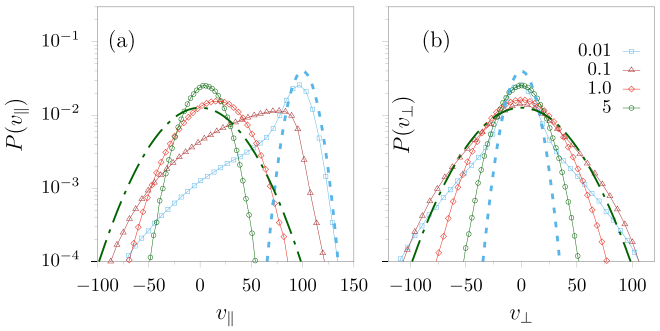

FIG. 1. Velocity distributions in the particle frame. Probability distributions of velocity components (a) parallel $P(v_\parallel)$ and (b) perpendicular $P(v_\perp)$ to the heading direction at Pe = 100 for various M values indicated in the common legend in (b). Similar to $P(v_\parallel)$, non-Gaussian long tails disappear in $P(v_\perp)$ at high inertia. In both plots, we compare the analytic distribution functions for noninteracting particles using Eq. (2) at $M = 0.01$ (dashed line) and $M = 5.0$ (dot-dashed line).

i.e., θ_i, undergoes a long-time diffusion, leading to an effective persistent motion. The inertial active dynamics evolve as

$$m\dot{\mathbf{v}}_i = -\gamma_t \mathbf{v}_i + \mathbf{F}_i + \mathbf{F}_{A,i} + \gamma_t\sqrt{2D_t}\,\eta_i(t),$$
$$I\ddot{\theta}_i = -\gamma_r\dot{\theta}_i + \gamma_r\sqrt{2D_r}\,\zeta_i(t), \tag{1}$$

where $\mathbf{F}_i = -\nabla_i \sum_j U(r_{ij})$, the symbols $\eta_i(t)$ and $\zeta_i(t)$ represent Gaussian white noises, and viscous drags associated with translation and rotation are described by $\gamma_t \mathbf{v}_i$ and $\gamma_r\dot{\theta}_i$, respectively. Interactions among particles are due to volume exclusion effects modeled via the Weeks-Chandler-Anderson potential: $U(r) = 4\epsilon[(\sigma/r)^{12} - (\sigma/r)^6] + \epsilon$ if the interparticle separation $r < r_c = 2^{1/6}\sigma$ and $U(r) = 0$ otherwise. The units of length and energy are set by σ and ϵ, respectively. The rotational diffusivity D_r can have a nonthermal active origin. Inertial relaxations in translation and rotation take time scales $\tau_I = m/\gamma_t$ and $\tau_d = I/\gamma_r$. Beyond τ_d, diffusion in the heading direction leads to a persistent motion with a bare persistence time $\tau_p = 1/D_r$, which sets the unit of time. Unless specified otherwise, we assume that particles are in contact with a thermal bath with $D_t = 1.0\,\sigma^2 D_r$, and a small and constant $\tau_d = 0.33\tau_p$ [24]. We particularly focus on the impact of changing activity in terms of the Péclet number $\mathrm{Pe} = v_0/(D_r\sigma)$ and that of the reduced mass using $M = \tau_I/\tau_p$. In order to fully characterize the properties of a homogeneous active bath, we fix the density to a low value, $\rho = 0.1$, corresponding to a packing fraction 8%, such that the system does not phase separate even in the overdamped limit [7].

III. RESULTS

An increase in Pe, as expected, drives the system away from equilibrium. In Fig. 1, we show the change in velocity distribution to reveal the impact of inertia. For this purpose, we consider the two components of the velocity, in the heading direction $v_\parallel = \mathbf{v}\cdot\hat{n}$ and perpendicular to it $v_\perp = (\mathbb{1} - \hat{n}\hat{n})\cdot\mathbf{v}$. In two dimensions, $v_\perp$ is a scalar. The distribution of velocity components $y = (v_\parallel, v_\perp)$ for noninteracting ABPs in the small and large M limits has the following Gaussian form

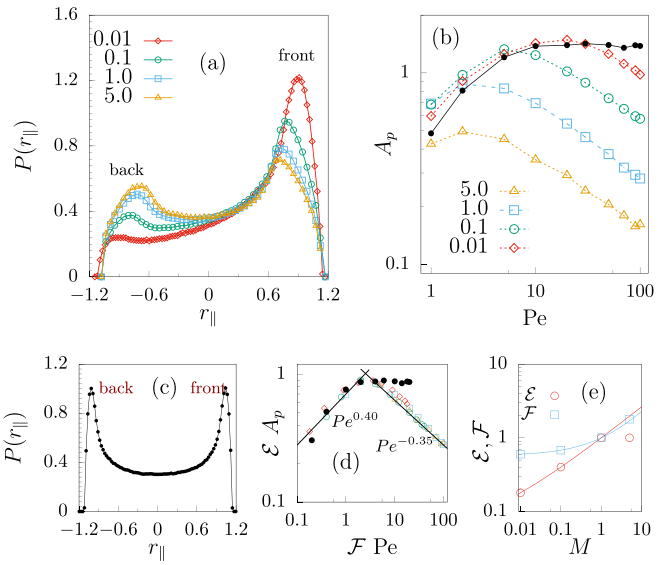

FIG. 2. Pair distribution in the heading direction: (a) $P(r_\parallel)$ at Pe = 100 and various M values indicated in the legend. The fore-aft asymmetry decreases with increasing M. One gets a fully symmetric distribution at equilibrium, as shown in (c). (b) Variation of asymmetry parameter A_p as a function of Pe is shown for various M values indicated in the legend. The black line connecting filled circles (•) represents overdamped dynamics. (d) An approximate data collapse is obtained for inertial systems using appropriate rescaling of (b). The filled circles (•) correspond to overdamped dynamics. (e) The variation of scale factors shown as a function of M. At large M, they show approximate dependencies $\mathcal{E} \sim M^{0.4}$ and $\mathcal{F} \sim M^{0.6}$.

(see Appendix A):

$$P(y) = \sqrt{\frac{M}{2\pi\tilde{D}}}\,e^{-\frac{M}{2\tilde{D}}(y-y_0)^2}. \tag{2}$$

Here, $y_0 = (\mathrm{Pe}, 0)$ and $\tilde{D} = 1$ for small $M \ll 1$. For large $M \gg 1$ one gets effective equilibriumlike behavior with $y_0 = (0, 0)$ and $\tilde{D} = D_{\mathrm{eff}}$ where $D_{\mathrm{eff}} = 1 + \mathrm{Pe}^2/2$. At small M, inertial lag is small. Despite that, $P(v_\parallel)$ for interacting ABPs at $M = 0.01$ shows a long tail reaching $v_\parallel < 0$. This tail, absent for noninteracting ABPs in Eq. (2), emerges due to enhanced frontal collision in the heading direction and the resultant inertial recoil. The asymmetry in collisions will be scrutinized using a pair distribution function in Fig. 2. At larger inertia, secondary back collisions become prominent, symmetrizing the distribution to a Gaussian-like profile, e.g., at $M = 5$ (see Appendix A for more details). The difference of Eq. (2) from numerical results is more subtle at $M = 5$. Although the distribution is Gaussian, the free particle estimate of D_{eff} fails to capture the observed behavior (Fig. 1) as for interacting ABPs D_{eff} reduces with M (Fig. 3). The $P(v_\perp)$ distribution also shows inertial restoration of equilibriumlike behavior [see Fig. 3(b)]. The long non-Gaussian tails are observable at small M and disappear with an increase in M. Bouncing backward and forward from neighboring particles at high inertia symmetrizes the distributions, rendering them equilibriumlike shapes. Comparison with Eq. (2) plotted with dashed lines highlights the difference in terms of the non-Gaussian tails at small M and a significant reduction of

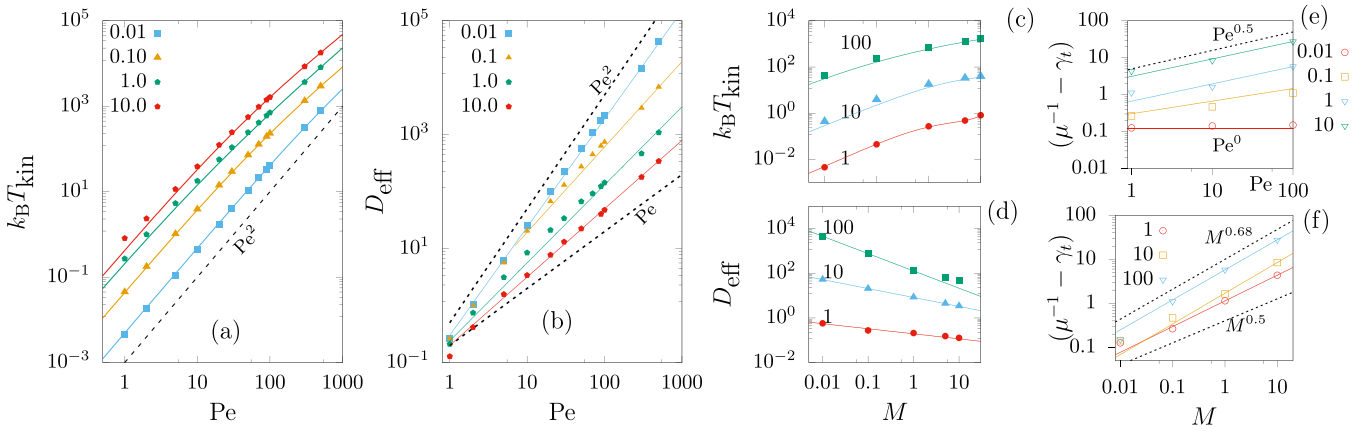

FIG. 3. Plots of dimensionless kinetic temperature $k_BT_{kin} = m\langle \mathbf{v}^2\rangle/2\epsilon$, effective diffusivity D_{eff}, and excess viscous drag $(\mu^{-1} - \gamma_t)$ with Pe at fixed M [legends in (a), (b), and (e)] and with M at fixed Pe [legends in (c), (d), and (f)]. The lines in (a) and (c) are fit with Eq. (C1). We use $\Pi_c \sim \mathrm{Pe}^{\alpha_1}$ with $\alpha_1 = 0.69, 0.66, 0.55, 0.67$ for $M = 0.01, 0.1, 1.0, 10$ in (a) and $\Pi_c \sim M^{\alpha_2}$ with $\alpha_2 = 2.5, 0.20, 0.50$ for $\mathrm{Pe} = 1, 10$, and 100 in (c). The black dashed line in (a) shows Pe^2 scaling expected for noninteracting ABPs. (b) Fits $D_{eff} \sim \mathrm{Pe}^{\alpha_d}$ with $\alpha_d = 1.98, 1.43, 1.13, 1.17$ at $M = 0.01, 0.1, 1, 5$ are shown. The two dashed lines indicate the upper and lower bounds of the scaling forms expected at small and large inertia. (d) Fits $D_{eff} \sim M^{-\gamma_d}$ with $\gamma_d = 0.27, 0.40, 0.78$ for $\mathrm{Pe} = 1$, 10, and 100. (e) For small M ($M = 0.01$), mobility is independent of Pe, as expected. In general, $(\mu^{-1} - \gamma_t) \sim \mathrm{Pe}^{\alpha_\mu}$ with $\alpha_\mu = 0.04, 0.34, 0.46, 0.47$ at $M = 0.01, 0.1, 1, 10$. The dotted line shows a $\mathrm{Pe}^{1/2}$ scaling. (f) $(\mu^{-1} - \gamma_t) \sim M^{\gamma_\mu}$ with $\gamma_\mu = 0.58, 0.69, 0.68$ at $\mathrm{Pe} = 1$, 10, 100.

D_{eff} at large M. The impact of interaction manifests in the pair-distribution function in the heading direction, i.e., the probability $P(r_\parallel)$ of finding a neighboring particle in direction $\hat{n}$ (see Fig. 2). Due to enhanced frontal collision, more particles accumulate in front. Such accumulations in front and associated depletion wakes have been analyzed recently in overdamped dilute ABPs [43,44]. A peak in the back appears due to secondary back collisions experienced by inertial ABPs after frontal recoil. With increasing M, recoil increases, reducing the frontal accumulation and increasing the secondary collisions from the back—these affect the symmetrization of the pair distribution—restoring equilibriumlike behavior.

The asymmetry in the pair distribution is quantified in terms of the parameter A_p that measures the difference between the heights of the front and back peaks [Fig. 2(b)]. For fixed M, the asymmetry initially increases with Pe. For overdamped systems (black solid line denoting $M = 0$), the increase is followed by saturation in the absence of recoil. In contrast, in the presence of inertia, after the initial increase, A_p decreases with Pe. The data collapse in Fig. 2(d) shows that at small Pe, the asymmetry increases with Pe as $A_p \sim \mathrm{Pe}^{0.4}$ and then decreases as $A_p \sim \mathrm{Pe}^{-0.35}$. Such scaling properties are common to all inertial ABPs. The increase is due to enhanced frontal collisions associated with increased activity. The decrease is due to inertial recoil and is the reason behind the restoration of equilibriumlike behavior.

Another way of measuring how far the system is from equilibrium is given by the extent to which the equilibrium Einstein relation is violated $\mathcal{I} = |D_{eff} - \mu\, k_BT_{kin}|$, where μ is the particle mobility and T_{kin} the so-called kinetic energy [45,46]. Following a tracer particle dynamics is a useful tool to characterize the properties of a bath [13,14,16,17,20,21]. In the presence of translational fluctuations, the impact of the activity on diffusivity at low Pe gets overshadowed by the thermal bath, i.e., D_t. While these effects can be subtracted out, for simplicity and intending to understand the impact of the activity, we set $D_t = 0$ in the following. From the late-time behavior of the mean-squared displacements, we obtain the effective diffusivity D_{eff}. The kinetic temperature k_BT_{kin} is readily obtainable from the velocity fluctuations. Using a separate numerical calculation of the change in velocity $\langle v_x\rangle$ of a test particle—that we consider to be another ABP particle, identical to ones that constitute the active fluid—under an external force f_x, we obtain the mobility $\mu = (\partial\langle v_x\rangle/\partial f_x)_{f_x=0}$ around the nonequilibrium steady states of the ABPs. In the presence of an external force on the test particle, a local statistical reorganization of other ABPs follows. Such a reorganization depends on active speed and inertia, resulting in the mobility variation. Using these, we obtain the violation $\mathcal{I}$.

In Fig. 3, we show the variations of kinetic temperature, diffusivity, and mobility as a function of Pe and M. We use a kinetic theory approach to develop an understanding of the observed behavior (see Appendix C 1). In the presence of interaction, the collision rate $\Pi_c \sim \Sigma\,\mathrm{Pe}$ with Σ denoting the collision cross section. For small mass, assuming soft recoil, we can use Maxwell approximation to get $\Sigma \sim \mathrm{Pe}^{-1}[(M + 1)/M]^{1/2}$ [47]. At large mass, a hard-core approximation gives $\Sigma \approx \sigma$. In general, one may use $\Pi_c \sim \mathrm{Pe}^{\alpha_1}M^{\alpha_2}$ with $\alpha_{1,2} > 0$. The mean-free time $\tau_f = \ell/\mathrm{Pe}$ with the mean-free path $\ell \approx 1/\rho\Sigma$. Thus, τ_f can be expressed in terms of the collision cross section as $\tau_f \sim (\rho\Pi_c)^{-1}$.

Using a recently derived expression for the dimensionless free ABP kinetic temperature $k_BT_{kin} = \frac{M\langle \mathbf{v}^2\rangle}{2\epsilon} = \frac{\mathrm{Pe}^2}{2}\frac{M}{M+1}$ [48], and including the observed decrease in kinetic temperature, we have the following phenomenological expression (Appendix C1):

$$k_BT_{kin} = \frac{\mathrm{Pe}^2}{2}\frac{M}{M + 1 + \mathcal{A}\,\rho\Pi_c}, \tag{3}$$

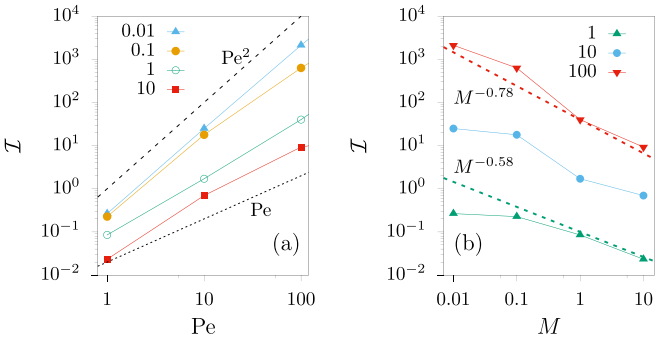

FIG. 4. The violation of equilibrium fluctuation dissipation $\mathcal{I} = |D_{\rm eff} - \mu k_B T_{\rm kin}|$, a measure of how far the system is from equilibrium as a function of Pe and M, is shown in (a) and (b), respectively. The fixed values of M and Pe at which the calculations are performed are denoted in legends of (a) and (b). $\mathcal{I}$ increases with Pe as Pe^{α_d}, where $\alpha_d = 2$ (at $M = 0.01$) and $\alpha_d = 1$ (for $M \geqslant 1$) give the upper and lower limits of the scaling form. At a given Pe, $\mathcal{I}$ decreases with increasing inertial mass M.

that exhibits a good fit to numerical results (Fig. 3). In addition, the expression suggests a low $k_B T_{\rm kin}$ at higher density, consistent with numerical observations in [24]. For free particles in two dimensions, the asymptotic active diffusivity $D_{\rm eff} = v_0^2/2D_r = \mathrm{Pe}^2/2$ and the inverse mobility $\mu^{-1} = \gamma_t$ are independent of M. When collisions dominate, $D_{\rm eff} \sim \ell\,\mathrm{Pe}$. Thus,

$$D_{\rm eff} \approx \begin{cases} \frac{1}{\rho}\mathrm{Pe}^2\left(\frac{M}{M+1}\right)^{1/2}, & M \ll 1 \\ \frac{1}{\rho\sigma}\mathrm{Pe}, & M \gg 1 \end{cases}. \tag{4}$$

In general, $D_{\rm eff} \sim Pe^{\alpha_d}$ and $D_{\rm eff} \sim M^{-\gamma_d}$ (Fig. 3). Equation (4) sets bounds on the Pe dependence in the two limits of M, showing good agreement with numerical results. Similarly, using mobility $\mu = \tau_f/M$, we find the following bounds on the excess viscous drag:

$$\mu^{-1} - \gamma_t \approx \begin{cases} \rho M, & M \ll 1 \\ \rho M \sigma \mathrm{Pe}, & M \gg 1 \end{cases}. \tag{5}$$

In general $[\mu^{-1} - \gamma_t] \sim \mathrm{Pe}^{\alpha_\mu}$ and M^{γ_μ}. The numerical results show $0 \leqslant \alpha_\mu < 1$ as per the bounds set in Eq. (5) (Fig. 3). However, numerically obtained values of γ_d and γ_μ are not well captured by Eqs. (4) and (5). For further details of the kinetic theory estimate, see Appendix C 1. Numerical estimates of mobility and diffusivity are discussed in Appendixes D and E. Moreover, the variations of the scaling exponents are shown in Appendix F.

With the help of the above results, we find that the violation $\mathcal{I}$ increases with Pe but decreases with M (Fig. 4). At small M, using kinetic theory estimates $D_{\rm eff} \sim \mathrm{Pe}^2$, $k_B T_{\rm kin} \sim \mathrm{Pe}^2$, and μ independent of Pe, we get $\mathcal{I} = |D_{\rm eff} - \mu\, k_B T_{\rm kin}| \sim \mathrm{Pe}^2$, which agrees approximately with the numerical results at $M = 0.01$. In the other limit of large inertia, again using kinetic theory estimates $D_{\rm eff} \sim \mathrm{Pe}$, $k_B T_{\rm kin} \sim \mathrm{Pe}^2$, and $\mu \sim \mathrm{Pe}^{-1}$, we get $\mathcal{I} \sim \mathrm{Pe}$ that again agrees approximately with numerical results at $M = 10$.

Moreover, $\mathcal{I}$ decreases with M. This can be described in terms of $D_{\rm eff} \sim M^{-\gamma_d}$ and $\mu \sim M^{-\gamma_\mu}$ and noting that $k_B T_{\rm kin}$ saturates at large M. Thus, one gets $\mathcal{I} \sim |M^{-\gamma_d} - M^{-\gamma_\mu}|$. With Pe, γ_d increases from 0.27 to 0.78 while γ_μ remains between 0.6 and 0.7. Thus, $\mathcal{I} \sim M^{-\gamma_\mu}$ with $\gamma_\mu = 0.58$ at $\mathrm{Pe} = 1$, and $\mathcal{I} \sim M^{-\gamma_d}$ with $\gamma_d = 0.78$ at $\mathrm{Pe} = 100$. These two scaling forms are shown using dashed lines in Fig. 4(b), and they capture the observed numerical results approximately.

In this paper, we kept a small and constant value for the rotational inertial time τ_d. One impact of the increase in τ_d can be an increase in the effective persistence time [49]. However, developing a detailed understanding of the impact of τ_d requires a separate in-depth study.

IV. CONCLUSION

We have shown how the nonequilibrium properties of an active fluid consisting of ABPs, at a density far away from the onset of MIPS, behave as a function of activity and inertial mass. While the departure from equilibrium gets pronounced with increasing Pe, i.e., activity, we found that inertial mass restores equilibriumlike properties. In particular, we showed that the non-Gaussian velocity distributions, the fore-aft asymmetry in the (heading-direction) pair distribution, and the absence of an Einstein fluctuation-dissipation relation between diffusivity, mobility, and kinetic temperature observed in active overdamped systems cross over to their equilibrium counterparts with inertial mass. In short, we found that the inertial recoil can effectively thermalize the active fluid, beyond the single-particle orientational relaxation over the inertial time scale. Remarkably, the late-time diffusivity and mobility of the bath depend on inertial mass, in contrast to free ABPs. The effective diffusivity and temperature grow with active velocity and decrease with inertial mass. In contrast, effective mobility decreases with mass and activity. Together, these findings show a reduction in the violation of equilibrium fluctuation dissipation with increasing inertia. In summary, inertia brings back equilibriumlike behavior in the active fluid.

ACKNOWLEDGMENTS

SAMKHYA, the high-performance computing facility at the Institute of Physics, Bhubaneswar, India, supported numerical calculations. D.C. thanks Arghya Majee for a critical reading of the first version of the paper; C. Y. Cergy Paris Université for a Visiting Professorship, which enabled the initiation of current work; SERB, India, for financial support through Grant No. MTR/2019/000750; and International Centre for Theoretical Sciences (ICTS-TIFR), Bangalore, India, for an Associateship. F.P. acknowledges financial support from C. Y. Initiative of Excellence (grant "Investissements d'Avenir," Grant No. ANR-16-IDEX-0008); INEX 2021 Ambition Project CollInt; and Labex MME-DII, Projects No. 2021-258 and No. 2021-297.

APPENDIX A: VELOCITY DISTRIBUTIONS

1. Free particle velocity distributions

Velocity distributions of noninteracting ABPs at small and large M limits are easy to find and have Gaussian profiles. At small M, the heading direction remains unchanged over the inertial relaxation time. Thus, velocity distributions in the free

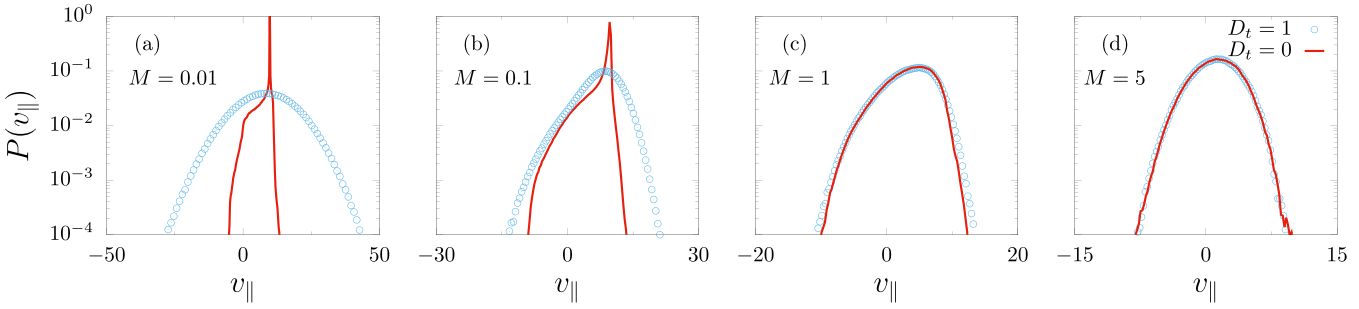

FIG. 5. Inertia brings back equilibriumlike features. The speed distributions in heading direction at Pe = 10 are shown for different masses $M = 0.01$ in (a), $M = 0.1$ in (b), $M = 1$ in (c), and $M = 5$ in (d). In each plot, blue points (red line) represent the results for $D_t = 1.0$ ($D_t = 0.0$).

particle limit are

$$P(v_\parallel) = \sqrt{M/2\pi}\,\exp[-(M/2)(v_\parallel - \mathrm{Pe})^2] \tag{A1}$$

and

$$P(v_\perp) = \sqrt{M/2\pi}\,\exp[-M\,v_\perp^2/2]. \tag{A2}$$

As is shown in Fig. 1, these distributions fail to capture the simulation results at $M = 0.01$, particularly the long non-Gaussian tail due to frontal collisions reaching $v_\parallel < 0$ values. In the large M limit, the heading direction can completely lose persistence over inertial relaxation, and one can use an effective equilibriumlike distribution:

$$P(v_\parallel) = \sqrt{M/2\pi D_{\mathrm{eff}}}\,\exp[-M v_\parallel^2/2D_{\mathrm{eff}}] \tag{A3}$$

and

$$P(v_\perp) = \sqrt{M/2\pi D_{\mathrm{eff}}}\,\exp[-M v_\perp^2/2D_{\mathrm{eff}}] \tag{A4}$$

with $D_{\mathrm{eff}} = 1 + \mathrm{Pe}^2/2$. While at $M = 5$, the numerical simulations do show Gaussian distributions, the difference from numerical results is more subtle. The free particle estimate of D_{eff} fails to capture the observed behavior (Fig. 1). As shown in Fig. 3, in the presence of interaction, D_{eff} reduces with M.

Finally, we note that Eqs. (A1)–(A4) agree with numerical simulations for free and inertial active Brownian particles in the small and large M limits [48].

2. Inertial thermalization

As has been pointed out in the main text, with increasing M, the velocity distribution gets thermalized due to collisions and recoil. Here we supplement that finding with an independent measure in which we compare the velocity distribution in the heading direction in the presence ($D_t = 1$) and absence ($D_t = 0$) of a thermal bath (Fig. 5). For small M, the two distributions are significantly different from each other. With increasing M, the distribution in the absence of thermal bath starts to *thermalize*, aided by relatively faster orientational relaxation of the heading direction during a slow inertial relaxation, and primarily due to collisions from the front and secondary collisions from back after the frontal recoil. As a result, they start to come close to each other to merge at $M \gtrsim 1$.

APPENDIX B: PAIR DISTRIBUTION

In Fig. 6, we show the distribution of particles around a test particle in its heading direction at Pe=1, 10, and 100 and inertia $M = 0, 0.01, 0.1, 1$. These distributions are used to calculate the asymmetry parameter A_p presented in the main text.

APPENDIX C: IMPACT OF INTERACTION—KINETIC THEORY ESTIMATES

Here, we adopt a kinetic theory argument to obtain approximate estimates of the changes due to interaction [47]. The collision rate $\Pi_c \sim \Sigma\,\mathrm{Pe}$ with Σ denoting the collision cross section (a length scale in two dimensions), which can be obtained by equating the kinetic and potential energies at collision. Assuming a power-law form for interaction energy

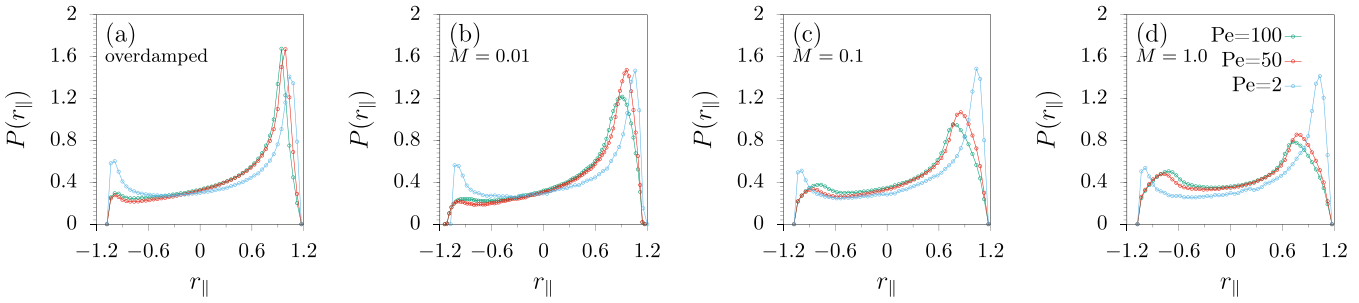

FIG. 6. Probability distribution of particle separation of interacting neighbors projected along the heading direction $P(r_\parallel)$ at the system density $\rho = 0.1$ for Pe = 2, 50, and 100. The results in (a) correspond to an overdamped system and in (b), (c), and (d) for an underdamped system with M values = 0.01, 0.1, and 1.0, respectively. The common legend representing different Pe values is placed inside plot (d).

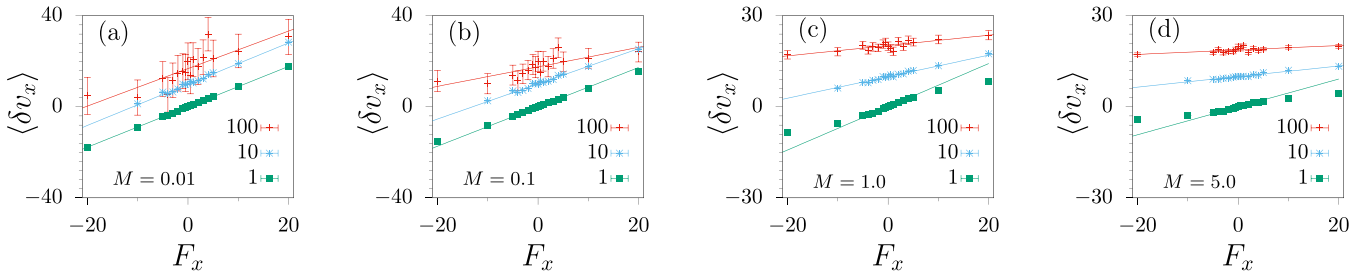

FIG. 7. The mean velocity of a tagged particle in response to the external force F_x is shown for Pe = 1, 10, and 100 in (a) at $M = 0.01$, in (b) at $M = 0.1$, in (c) at $M = 1.0$, and in (d) at $M = 5$. The slope of the corresponding linear fits at $F_x = 0$ gives mobility $\mu = \lim_{F_x \to 0} \langle \delta v_x \rangle / F_x$. By definition $\langle \delta v_x \rangle = 0$ at $F_x = 0$. For the sake of clear visualization, each curve for Pe = 10 and 100 is shifted upwards.

$U(r) \sim r^{-\nu}$, and the free-particle estimate of kinetic temperature presented above, $\Sigma \sim \mathrm{Pe}^{-2/\nu}[(M+1)/M]^{1/\nu}$. Thus,

$$\Pi_c \sim \mathrm{Pe}^{1-2/\nu}[(M+1)/M]^{1/\nu}.$$

Within the Maxwell approximation [47], Π_c is independent of Pe requiring $\nu = 2$, i.e., $\Sigma \sim \mathrm{Pe}^{-1}[(M+1)/M]^{1/2}$. Such a *soft-core* approximation can work for relatively small mass and slower recoil. For faster recoil at large mass, a hard-core approximation gives $\Sigma \approx \sigma$ and thus $\Pi_c \approx \sigma \mathrm{Pe}$. In general, one may use $\Pi_c \sim \mathrm{Pe}^{\alpha_1} M^{\alpha_2}$ with $\alpha_{1,2} > 0$.

1. Kinetic temperature

In the presence of interaction, $k_B T_{\mathrm{kin}}$ gets suppressed due to collisions. This can be incorporated using the dimensionless collision rate $\tau_p/\tau_f \sim \rho \Pi_c$ such that $k_B T_{\mathrm{kin}} = \frac{\mathrm{Pe}^2}{2} \frac{M}{M+1+(\tau_p/\tau_f)}$. Thus, we use the following phenomenological expression:

$$k_B T_{\mathrm{kin}} = \frac{\mathrm{Pe}^2}{2} \frac{M}{M+1+\mathcal{A}\rho\Pi_c}. \tag{C1}$$

2. Diffusivity

Within the kinetic theory, assuming frequent collisions over the persistence time τ_p, collisions mainly govern the change in velocity direction. Thus one can write $D_{\mathrm{eff}} \sim \ell\, \mathrm{Pe}$, where the mean free path $\ell \sim 1/\rho\Sigma$, leading to

$$D_{\mathrm{eff}} \approx \frac{1}{\rho} \mathrm{Pe}^{1+2/\nu} \left[\frac{M}{M+1}\right]^{1/\nu} \tag{C2}$$

such that

$$D_{\mathrm{eff}} \approx \frac{1}{\rho} \mathrm{Pe}^2 \left(\frac{M}{M+1}\right)^{1/2}$$

within Maxwell approximation at small M and

$$D_{\mathrm{eff}} \approx \frac{1}{\rho\sigma} \mathrm{Pe}$$

independent of M at large M. These estimates qualitatively agree with the Pe dependence of numerical results. However, explanation of the detailed power-law dependencies $D_{\mathrm{eff}} \sim Pe^{\alpha_d}$ and $M^{-\gamma_d}$ observed from simulations remains outside the scope of such simple explanation.

3. Mobility

Under external force F on a particle, its acceleration F/m can increase the velocity for a duration τ_f, the mean free time before the next collision. Thus the drift velocity $v_d = (F/m)\tau_f = \mu F$ with mobility $\mu = \tau_f/m$. The equilibrium bath provides an additional viscous friction coefficient γ_t. Now for the active system $\tau_f = \ell/\mathrm{Pe} = 1/\rho\Sigma\mathrm{Pe}$. At small M, using the soft-core Maxwell estimate $\Sigma\mathrm{Pe} = 1$, we get

$$\mu^{-1} - \gamma_t = M/\tau_f \approx \rho M \tag{C3}$$

independent of Pe. At large M, the hard-core approximation $\Sigma = \sigma$ gives

$$\mu^{-1} - \gamma_t = M/\tau_f \approx \rho M\, \sigma \mathrm{Pe}. \tag{C4}$$

This suggests, in general, that $[\mu^{-1} - \gamma_t] \sim \mathrm{Pe}^{\alpha_\mu}$ with $0 \leqslant \alpha_\mu < 1$. The numerical results in Fig. 3(e) remain within these bounds. However, the M dependence in Fig. 3(f) shows more

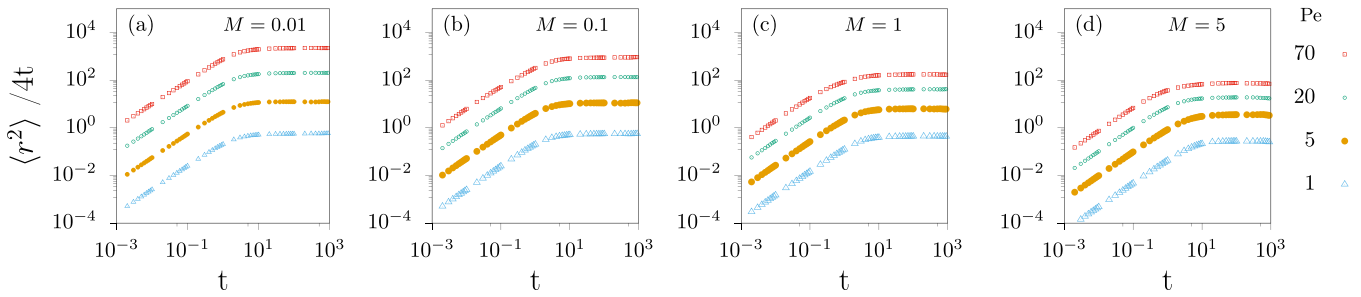

FIG. 8. Mean square displacement for Pe = 1, 5, 20, and 70 in (a) at $M = 0.01$, in (b) at $M = 0.1$, in (c) at $M = 1.0$, and in (d) at $M = 5$. The common legend representing different Pe values is placed at the extreme right. These calculations are done for $D_t = 0$.

complex power-law growth in the viscous drag $[\mu^{-1} - \gamma_t] \sim M^{\gamma_\mu}$ unlike the linear estimate obtained from the above kinetic theory estimates.

APPENDIX D: MOBILITY FROM SIMULATIONS

To measure mobility, we apply an additional force F_x on the tagged particle and calculate its mean velocity along the same direction $\langle v_x \rangle$ for various F_x values. The mean velocity $\langle \delta v_x \rangle = \langle v_x \rangle|_{F_x>0} - \langle v_x \rangle|_{F_x=0}$ as a function of F_x is shown in Fig. 7. The slope of the linear fit for $\langle \delta v_x \rangle$ vs F_x curve near $F_x = 0$ gives mobility. In the overdamped regime $M = 0.01$, mobility does not show dependency on Pe as its value is observed to be the same: $\mu \approx 0.9$ for Pe $= 1$, 10, and 100 Fig. 7(a). In the underdamped limit ($M \geqslant 0.1$), mobility decreases with Pe [see Figs. 7(b)–7(d)].

APPENDIX E: MEAN-SQUARED DISPLACEMENT

In Fig. 8, we plot mean-squared displacement $\langle r^2 \rangle$ scaled by time t for different M and Pe values. All of them show ballistic to diffusive crossover at a time scale determined by the orientational persistence of the heading direction, a quantity that is kept constant in this paper. The asymptotic diffusivities $D_{\text{eff}} = \lim_{t\to\infty} \langle \mathbf{r}^2 \rangle / 4t$ are obtained from these graphs and used in the main text.

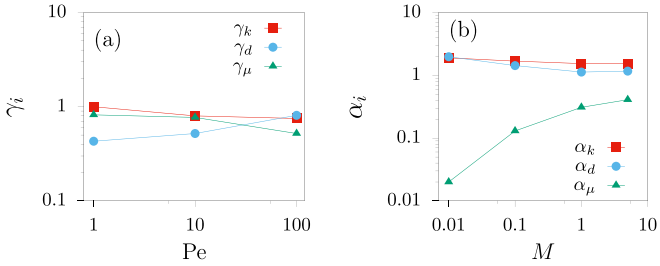

FIG. 9. Scaling exponents γ_i and α_i used in Fig. 4 are presented as a function of Pe (a) and M (b), respectively. $i = k, d, \mu$ represent exponents of kinetic energy, diffusion, and mobility.

APPENDIX F: SCALING EXPONENTS

The variations of scaling exponents determining the Pe and M dependence of kinematic temperature, effective diffusivity, and mobility are shown in Fig. 9.

[1] P. M. Chaikin and T. C. Lubensky, *Principles of Condensed Matter Physics* (Cambridge University, Cambridge, England, 2012).

[2] C. Bechinger, R. Di Leonardo, H. Löwen, C. Reichhardt, G. Volpe, and G. Volpe, Active particles in complex and crowded environments, Rev. Mod. Phys. **88**, 045006 (2016).

[3] M. C. Marchetti, J. F. Joanny, S. Ramaswamy, T. B. Liverpool, J. Prost, M. Rao, and R. A. Simha, Hydrodynamics of soft active matter, Rev. Mod. Phys. **85**, 1143 (2013).

[4] P. Romanczuk, M. Bär, W. Ebeling, B. Lindner, and L. Schimansky-Geier, Active Brownian particles, Eur. Phys. J. Spec. Top. **202**, 1 (2012).

[5] S. Ramaswamy, Active fluids, Nat. Rev. Phys. **1**, 640 (2019).

[6] G. Gompper, R. G. Winkler, T. Speck, A. Solon, C. Nardini, F. Peruani, H. Löwen, R. Golestanian, U. B. Kaupp, L. Alvarez, T. Kiørboe, E. Lauga, W. C. K. Poon, A. DeSimone, S. Muiños-Landin, A. Fischer, N. A. Söker, F. Cichos, R. Kapral, P. Gaspard, *et al.*, The 2020 motile active matter roadmap, J. Phys.: Condens. Matter **32**, 193001 (2020).

[7] D. Richard, H. Löwen, and T. Speck, Nucleation pathway and kinetics of phase-separating active Brownian particles, Soft Matter **12**, 5257 (2016).

[8] X. L. Wu and A. Libchaber, Particle diffusion in a quasi-two-dimensional bacterial bath, Phys. Rev. Lett. **84**, 3017 (2000).

[9] G. Grégoire, H. Chaté, and Y. Tu, Comment on "Particle diffusion in a quasi-two-dimensional bacterial bath," Phys. Rev. Lett. **86**, 556 (2001).

[10] A. Jepson, V. A. Martinez, J. Schwarz-Linek, A. Morozov, and W. C. K. Poon, Enhanced diffusion of nonswimmers in a three-dimensional bath of motile bacteria, Phys. Rev. E **88**, 041002(R) (2013).

[11] G. Miño, T. E. Mallouk, T. Darnige, M. Hoyos, J. Dauchet, J. Dunstan, R. Soto, Y. Wang, A. Rousselet, and E. Clement, Enhanced diffusion due to active swimmers at a solid surface, Phys. Rev. Lett. **106**, 048102 (2011).

[12] J. M. Lahtinen, T. Hjelt, T. Ala-Nissila, and Z. Chvoj, Diffusion of hard disks and rodlike molecules on surfaces, Phys. Rev. E **64**, 021204 (2001).

[13] S. Ye, P. Liu, F. Ye, K. Chen, and M. Yang, Active noise experienced by a passive particle trapped in an active bath, Soft Matter **16**, 4655 (2020).

[14] C. Maes, Fluctuating motion in an active environment, Phys. Rev. Lett. **125**, 208001 (2020).

[15] C. Maes, Response theory: A trajectory-based approach, Front. Phys. **8**, 229 (2020).

[16] O. Granek, Y. Kafri, and J. Tailleur, Anomalous transport of tracers in active baths, Phys. Rev. Lett. **129**, 038001 (2022).

[17] P. Rizkallah, A. Sarracino, O. Bénichou, and P. Illien, Microscopic theory for the diffusion of an active particle in a crowded environment, Phys. Rev. Lett. **128**, 038001 (2022).

[18] E. W. Burkholder and J. F. Brady, Tracer diffusion in active suspensions, Phys. Rev. E **95**, 052605 (2017).

[19] J. Stenhammar, C. Nardini, R. W. Nash, D. Marenduzzo, and A. Morozov, Role of correlations in the collective behavior of microswimmer suspensions, Phys. Rev. Lett. **119**, 028005 (2017).

[20] V. Démery, O. Bénichou, and H. Jacquin, Generalized Langevin equations for a driven tracer in dense soft colloids: Construction and applications, New J. Phys. **16**, 053032 (2014).

[21] V. Démery and D. S. Dean, Perturbative path-integral study of active- and passive-tracer diffusion in fluctuating fields, Phys. Rev. E **84**, 011148 (2011).

[22] D. Loi, S. Mossa, and L. F. Cugliandolo, Effective temperature of active complex matter, Soft Matter **7**, 3726 (2011).
[23] L. F. Cugliandolo, G. Gonnella, and I. Petrelli, Effective temperature in active Brownian particles, Fluct. Noise Lett. **18**, 1940008 (2019).
[24] S. Mandal, B. Liebchen, and H. Löwen, Motility-induced temperature difference in coexisting phases, Phys. Rev. Lett. **123**, 228001 (2019).
[25] J. Reichert and T. Voigtmann, Tracer dynamics in crowded active-particle suspensions, Soft Matter **17**, 10492 (2021).
[26] E. W. Burkholder and J. F. Brady, Nonlinear microrheology of active Brownian suspensions, Soft Matter **16**, 1034 (2020).
[27] I. Petrelli, L. F. Cugliandolo, G. Gonnella, and A. Suma, Effective temperatures in inhomogeneous passive and active bidimensional Brownian particle systems, Phys. Rev. E **102**, 012609 (2020).
[28] L. Caprini and U. Marini Bettolo Marconi, Active matter at high density: Velocity distribution and kinetic temperature, J. Chem. Phys. **153**, 184901 (2020).
[29] C. Reichhardt and C. J. Olson Reichhardt, Active microrheology in active matter systems: Mobility, intermittency, and avalanches, Phys. Rev. E **91**, 032313 (2015).
[30] Y. Fily and M. C. Marchetti, Athermal phase separation of self-propelled particles with no alignment, Phys. Rev. Lett. **108**, 235702 (2012).
[31] G. S. Redner, M. F. Hagan, and A. Baskaran, Structure and dynamics of a phase-separating active colloidal fluid, Phys. Rev. Lett. **110**, 055701 (2013).
[32] C. B. Caporusso, P. Digregorio, D. Levis, L. F. Cugliandolo, and G. Gonnella, Motility-induced microphase and macrophase separation in a two-dimensional active Brownian particle system, Phys. Rev. Lett. **125**, 178004 (2020).
[33] C. Scholz, S. Jahanshahi, A. Ldov, and H. Löwen, Inertial delay of self-propelled particles, Nat. Commun. **9**, 5156 (2018).
[34] H. Löwen, Inertial effects of self-propelled particles: From active Brownian to active Langevin motion, J. Chem. Phys. **152**, 040901 (2020).
[35] M. Sandoval, Pressure and diffusion of active matter with inertia, Phys. Rev. E **101**, 012606 (2020).
[36] P. Herrera and M. Sandoval, Maxwell-Boltzmann velocity distribution for noninteracting active matter, Phys. Rev. E **103**, 012601 (2021).
[37] L. Hecht, S. Mandal, H. Löwen, and B. Liebchen, Active refrigerators powered by inertia, Phys. Rev. Lett. **129**, 178001 (2022).
[38] A. Solon and J. M. Horowitz, On the Einstein relation between mobility and diffusion coefficient in an active bath, J. Phys. A **55**, 184002 (2022).
[39] M. te Vrugt, T. Frohoff-Hülsmann, E. Heifetz, U. Thiele, and R. Wittkowski, From a microscopic inertial active matter model to the Schrödinger equation, Nat. Commun. **14**, 1302 (2023).
[40] O. Dauchot and V. Démery, Dynamics of a self-propelled particle in a harmonic trap, Phys. Rev. Lett. **122**, 068002 (2019).
[41] C. Scholz, M. Engel, and T. Pöschel, Rotating robots move collectively and self-organize, Nat. Commun. **9**, 931 (2018).
[42] A. Deblais, T. Barois, T. Guerin, P.-H. Delville, R. Vaudaine, J. S. Lintuvuori, J.-F. Boudet, J.-C. Baret, and H. Kellay, Boundaries control collective dynamics of inertial self-propelled robots, Phys. Rev. Lett. **120**, 188002 (2018).
[43] A. Poncet, O. Bénichou, V. Démery, and D. Nishiguchi, Pair correlation of dilute active Brownian particles: From low-activity dipolar correction to high-activity algebraic depletion wings, Phys. Rev. E **103**, 012605 (2021).
[44] J. K. G. Dhont, G. W. Park, and W. J. Briels, Motility-induced inter-particle correlations and dynamics: A microscopic approach for active Brownian particles, Soft Matter **17**, 5613 (2021).
[45] V. Blickle, T. Speck, C. Lutz, U. Seifert, and C. Bechinger, Einstein relation generalized to nonequilibrium, Phys. Rev. Lett. **98**, 210601 (2007).
[46] D. Chaudhuri and A. Chaudhuri, Modified fluctuation-dissipation and Einstein relation at nonequilibrium steady states, Phys. Rev. E **85**, 021102 (2012).
[47] P. L. Krapivsky, S. Redner, and E. Ben-Naim, *A Kinetic View of Statistical Physics* (Cambridge University, Cambridge, England, 2010).
[48] M. Patel and D. Chaudhuri, Exact moments and re-entrant transitions in the inertial dynamics of active Brownian particles, New J. Phys. **25**, 123048 (2023).
[49] L. Caprini, R. K. Gupta, and H. Löwen, Role of rotational inertia for collective phenomena in active matter, Phys. Chem. Chem. Phys. **24**, 24910 (2022).